Coherent Tunneling Transport in Molecular Junctions†

Hyunwook Song,‡ Youngsang Kim,§,|| Heejun Jeong,§ Mark A. Reed,*,⊥ and Takhee Lee*,‡

Department of Nanobio Materials and Electronics, Department of Materials Science and Engineering, Gwangju Institute of Science and Technology, Gwangju 500-712, Korea, Department of Applied Physics, Hanyang University, Ansan 426-791, Korea, and Departments of Electrical Engineering and Applied Physics, Yale University, New Haven, Connecticut 06520

Received: May 24, 2010; Revised Manuscript Received: August 10, 2010

Using saturated alkyl chain series with a dithiol anchor group, we systematically examined the intrinsic charge transport of single-molecule junctions in an electromigrated nanogap electrode. The saturated alkyl molecular system constitutes an important control series in molecular transport experiments to corroborate valid molecular junctions, because molecular energy levels remain nearly unchanged with molecular length, and the transport mechanism has been unambiguously established. Inelastic electron tunneling spectroscopy, temperature-variable current−voltage measurement, length-dependent conductance measurement, and transition voltage spectroscopy all validate the observation of intrinsic molecular properties in the electromigrated nanogap junctions.

Introduction

Since Aviram and Ratner proposed the first molecular rectifier to predict the feasibility of constructing a functional molecular device with using single molecules as active elements,[1] the field of molecular electronics has attracted a lot of interest over the past few decades.[2,3] A diversity of characteristic functions illustrated by single molecules, including rectifiers,[4] switches,[5] and transistors,[6−8] have been accordingly designed and reported. All these aspects render single molecules as promising candidates for the next generation of electronics. Furthermore, it is now possible to measure charge transport through single molecules or small molecular groups bridging macroscopic external contacts with the rapid development of various measuring techniques. For example, the electromigrated nanogap is one of a number of widely adopted techniques to achieve electrical contacts to single or very few molecules, and which is especially advantageous to prepare three-terminal molecular devices.[6,7] The fabrication is performed by the controlled passage of a large electrical current through the thin metal wire predefined by electron-beam lithography, causing the electromigration of metal atoms and eventual breakage of the metal wire.[9] This process can yield a stable electrode separation with a nanometer-sized gap, which is often bridged by the desired molecules, creating molecular transport junctions.

In this study, we present the characterization of coherent tunneling transport in the molecular junction formed by the electromigrated nanogap using a series of alkanedithiol molecules having various lengths, in combination with a variety of molecular transport techniques including inelastic electron tunneling spectroscopy (IETS),[10−12] temperature- and length-variable transport measurements,[13] and transition voltage spectroscopy (TVS).[14−16] The alkanedithiols constitute a prototypical control series in molecular transport experiments, because their effective energy levels remain to be almost invariant with molecular length, and it has been clearly demonstrated that coherent, off-resonant tunneling is the transport mechanism for these molecular junctions.[13,17] Thus, they form a perfect control to corroborate intrinsic molecular properties in the electromigrated nanogap junctions, letting us firmly exclude not only defective features arising from the possible metal (or impurity) debris in the gap after fabrication[18−23] but also the formation of tunnel junctions without the desired molecules.[16,24]

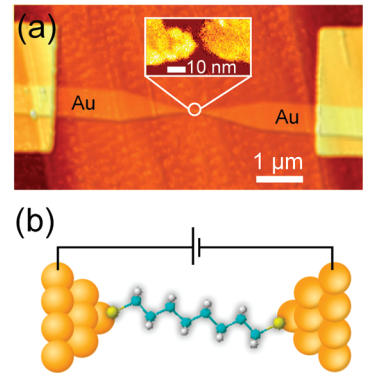

Figure 1. (a) Atomic force microscopy image of continuous Au wire before electromigration. The inset shows a false colored scanning electron microscopy image focusing on a broken nanogap after electromigration. (b) A schematic of a final device incorporating a 1,8-octanedithiol molecule into the electromigrated nanogap junction.

Experimental Methods

Device Fabrication. Electron-beam lithography and lift-off are used to create 15-nm-thick Au wires with widths of about 50 nm at their narrowest constriction, as shown in Figure 1a. After the samples were cleaned in oxygen plasma for 1 min, molecular deposition on the Au surface was performed in a dilute solution (1 mM) of alkanedithiol molecules in 10 mL of ethanol for 24 h, inside a nitrogen-filled glovebox with an oxygen level of less than 10 ppm. Before use, each sample was rinsed in ethanol and gently blown dry in a nitrogen stream to remove noncovalently attached molecules. Then, the samples

† Part of the "Mark A. Ratner Festschrift".

* To whom correspondence should be addressed. E-mail: tlee@gist.ac.kr (T.L.); mark.reed@yale.edu (M.A.R.).

‡ Gwangju Institute of Science and Technology.

§ Hanyang University.

|| Present address: Department of Physics, University of Konstanz, D-78457 Konstanz, Germany.

⊥ Yale University.

10.1021/jp104760b
Published on Web 08/26/2010

coated with the molecules were immediately cooled down to 4.2 K (in a vacuum cryostat), and the electromigration proceeded to form electrode pairs with a nanometer-scale separation by ramping up a dc voltage,[9,25] across which the molecules are attached. The schematic of the final devices is illustrated in Figure 1b.

Low Temperature Transport and IETS Measurements. The transport and IETS measurements of the electromigrated molecular junctions were performed at 4.2 K, with a custom-built cryogenic measurement apparatus. The devices are mounted onto a 28-pin leadless chip carrier socket on the sample stage inside a vacuum chamber that is evacuated and purged with He gas before being lowered into a liquid He storage dewar. In order to reduce the noise level, triaxial cables are used to connect the socket leads to the measurement instruments outside the cryogenic vacuum chamber through vacuum electrical feed-throughs. A calibrated Lakeshore thermometer is mounted on the sample stage to monitor sample temperature, and a resistive heater in a feedback loop with the thermometer is mounted on the sample stage to maintain the sample temperature. In order to measure the current (I)−voltage (V) characteristics, we used a 16-bit digital-to-analog converter for bias voltages and a low-noise current amplifier (Ithaco 1211) followed by a digital multimeter (Agilent 34410) for current measurement. All the grounds of the system were isolated to remove ground-loops and electrical noise. The IETS (d^2I/dV^2) spectrum was directly measured using a lock-in amplifier (Stanford Research Systems 830) and a home-built current−voltage sweeper controlled by a computer running via GPIB. An ac modulation of 7.8 mV (root-mean-square) at a frequency of 1033 Hz with a lock-in time constant of 1 s was applied to the sample to obtain the second harmonic signals, proportional to d^2I/dV^2. The ac modulation voltage is added to a dc bias generated by the 16-bit digital-to-analog converter, using operational amplifier-based custom circuitry.[26] Note that such a direct measurement of the second harmonic signal is preferential to numerical differentiation of the dI/dV data because the numerical differentiation decreases the signal-to-noise ratio.

Results and Discussion

In the process of breaking the Au wire, the molecules covering the surface of the initial Au wire occasionally become trapped in the junction. The molecular trapping events between the separated gap electrodes are not controllable but inherently stochastic.[27] In this study, we examined more than 800 nanogap devices, and then we focused on 42 (~5%) devices showing a reproducible symmetry $I(V)$ curve with a sigmoid shape, indicative of a typical coherent tunneling feature. In the following sections, we demonstrate the molecular contribution to charge transport in these junctions by performing a variety of transport techniques by which we can establish criteria to constitute valid single or few molecule junctions. The remaining 26% devices showed Coulomb blockade or zero-bias enhancement of the conductance indicative of the Kondo effect, most likely where small islands in the form of gold grains are present in the gap region instead of molecules.[19,20,23,27] In about 40% of the devices, no detectable current was observed (electrodes too far apart for measurable conduction). In addition, the remainder of the devices were too unstable to study the transport characteristics in detail. For example, current-induced irreversible changes take place and device stability is often poor at high current densities and elevated temperatures significantly above 4.2 K, likely owing to the atomic diffusion of the Au electrode materials.[22] These unstable devices were regarded as nonworking devices as well.

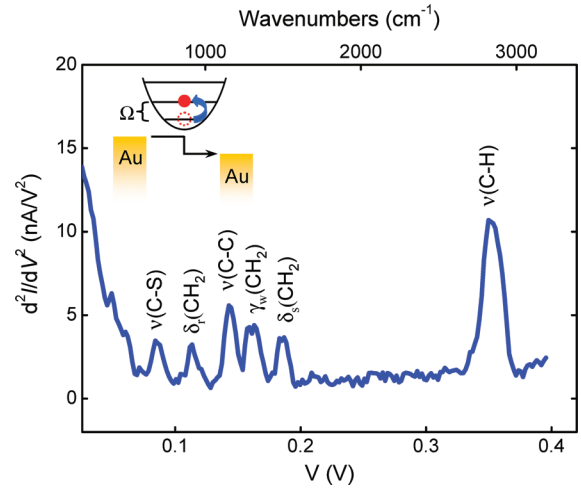

Figure 2. IETS spectrum (d^2I/dV^2) of Au−1,8-octanedithiol−Au junctions, directly obtained from the lock-in second harmonic signal at 4.2 K. The peaks are labeled with their assigned vibrational modes (see also Table 1). The inset shows an energy diagram illustrating the inelastic tunneling process. An inelastic tunneling channel is open at the excitation threshold $|eV| = \Omega$ for a molecular vibration.

TABLE 1: Summary of Vibrational Mode Assignments for the IETS Spectrum of Au−1,8-Octanedithiol−Au Junctions

peak position			
in mV	in cm^{-1}	mode assignment	description
84	677	ν(C−S)	C−S stretching
113	911	$\delta_r(CH_2)$	CH_2 in-plane rocking
142	1145	ν(C−C)	C−C stretching
159	1282	$\gamma_w(CH_2)$	CH_2 out-of-plane wagging
186	1500	$\delta_s(CH_2)$	CH_2 in-plane scissoring
353	2847	ν(C−H)	C−H stretching

Inelastic Electron Tunneling Spectroscopy. Inelastic electron tunneling spectroscopy (IETS) has recently become a primary characterization technique to identify the component molecules present in molecular transport junctions,[6,10−12] analogous to infrared and Raman spectroscopy for macroscopic samples, for an unambiguous determination of the molecular species in the junction. In IETS, as illustrated in the inset of Figure 2, an inelastic tunneling channel can be open, in addition to the elastic one, above the excitation threshold $|eV| = \Omega$ for a molecular vibration (where e is elementary charge, V is applied bias, and Ω is vibrational energy).[28] The conductance change caused by the opening of the inelastic channel at $|eV| = \Omega$ is very small (<1%) in generic off-resonant conditions which are situated in the limit of weak coupling between the transporting charge and the frontier molecular orbitals, and thus is usually not visible in $I(V)$ plots.[28] Instead, such changes can be clearly observed as reproducible features (usually peaks) in the second derivative d^2I/dV^2 plotted against V.

Figure 2 shows a representative IETS spectrum of Au−1,8-octanedithiol−Au junctions. A standard ac modulation technique with a lock-in amplifier was carried out at 4.2 K to directly acquire the second (d^2I/dV^2) harmonic signals (see the above Experimental Section for details). The spectra are stable and reproducible upon successive bias sweep, and the same vibrational peaks are observed repetitively for other octanedithiol junctions. The antisymmetry for positive and negative bias in the IETS spectrum is also checked in Figure S1 (in the Supporting Information), using a different octanedithiol junction. We assign the observed spectral features to specific molecular vibrations by comparison with previously reported infrared, Raman, and IETS measurements, and also by density functional

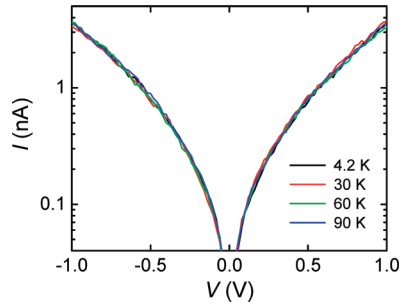

Figure 3. Semilog plot of temperature-variable $I(V)$ characteristics for Au−1,8-octanedithiol−Au junctions at selected temperatures (4.2, 30, 60, and 90 K).

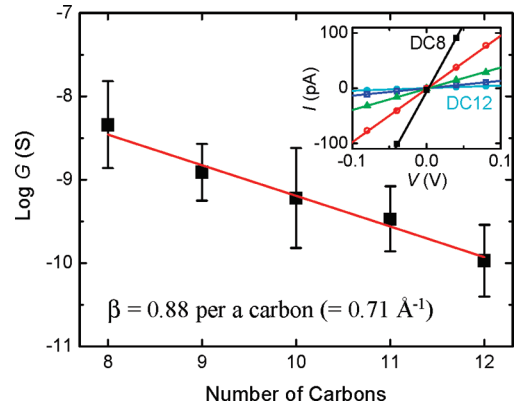

Figure 4. Semilog plot of the conductance versus the number of carbon atoms for five different length alkanedithiol nanogap junctions. The decay coefficient (β) can be determined from the linear fit (the solid line), yielding a β value of 0.88 (=0.71 Å^{-1}) per carbon atom assuming a through-bond tunneling. The average conductance values and standard deviations for the selected data are also given in Figure S2 (in the Supporting Information). The inset shows length-dependent $I(V)$ curves in the low-bias linear regime, where a conductance value is obtained from linear fits to the data.

theory calculations. In the IETS spectrum, peaks are reproducibly observed at 84, 113, 142, 159, 186, and 353 mV, which correspond to ν(C−S) stretching, δ_r(CH$_2$) rocking, ν(C−C) stretching, γ_w(CH$_2$) wagging, δ_s(CH$_2$) scissoring, and ν(C−H) stretching modes, respectively. The absence of a prominent peak corresponding to the ν(S−H) stretching mode at ∼319 mV (2575 cm^{-1}) indicates that the thiol (−SH) anchoring group is reacted with the Au electrode pairs broken during the electromigration.[10] The detailed peak assignments for molecular vibrations observed in this study are listed in Table 1. All of the spectral features are attributable to vibrational modes associated with the molecular species, which suggests that the molecule is the only thing in the junction through which tunneling is occurring. Therefore, the fully assigned IETS spectrum provides unambiguous experimental evidence of the existence of the constituent molecules incorporated into the electromigrated nanogap junctions.

Temperature- and Length-Variable Transport Measurements. The temperature-variable $I(V)$ measurement is necessary to investigate the conduction mechanism. Figure 3 shows a representative temperature-variable $I(V)$ characteristic of 1,8-octanedithiol bridging the Au nanogap electrodes as described in Figure 1. The $I(V)$ curves were measured between 4.2 and 90 K, and no temperature dependence was observed. The temperature-independent $I(V)$ characteristic is a clear manifestation of tunneling, and eliminates many of the other potential alternative mechanisms such as thermionic or hopping conductions. Thus far, a consistent picture has emerged for the off-resonant tunneling mechanism with saturated alkyl chains,[13] which can be reasonably expected when the Fermi energy of the electrode lies within a large energy gap between the highest occupied molecular orbital (HOMO) and the lowest unoccupied molecular orbital (LUMO) of short molecules as in the case of alkanedithiols.

Another well-established validation method to interrogate the transport mechanism of molecular junctions is to examine the dependence of conductance on the molecular length.[29−31] For example, in the case of coherent, off-resonant tunneling, the conductance of alkanedithiol molecules will show an exponential decrease with the molecular length. In particular, the conductance (G) is expected to be proportional to exp($-\beta N$), where N is the number of carbon atoms in alkanedithiol molecules and β is the tunneling decay coefficient. In order to investigate the length-dependent conductance, we examined the conductance of five different alkanedithiols with various chain lengths: 1,8-octanedithiol (HS−C$_8$H$_{16}$−SH, denoted as DC8 for the number of carbon atoms), 1,9-nonanedithiol (HS−C$_9$H$_{18}$−SH, DC9), 1,10-decanedithiol (HS−C$_{10}$H$_{20}$−SH, DC10), 1,11-undecanedithiol (HS−C$_{11}$H$_{22}$−SH, DC11), and 1,12-dodecanedithiol (HS−C$_{12}$H$_{24}$−SH, DC12). As illustrated in the inset of Figure 4, the conductance values were obtained by the least-squares linear fit from low-bias regimes (-0.1 V $\leq V \leq$ 0.1 V) of $I(V)$ characteristics. As anticipated above, we see that a semilog plot of the conductance values versus the molecular length is linear in Figure 4. Each conductance value in Figure 4 represents the average of data selected with the one sigma criteria (see Figure S2 in the Supporting Information for details of the data selection), and the error bar is the standard deviation for the selected data. From the linear fit (the solid line across data points) in Figure 4, we found a β value of 0.88 (=0.71 Å^{-1}) per carbon atom assuming a through-bond tunneling. This β value is in good agreement with the previously reported values in the literature.[13,29−31] Consequently, the correct exponential decrease of conductance upon a molecular length increase, temperature dependence of $I(V)$ characteristics, and agreement with decay coefficients all point to a valid molecular junction.

Transition Voltage Spectroscopy. Transition voltage spectroscopy (TVS) is a very promising method as a spectroscopic tool for molecular transport junctions.[14−16,32−34] Initially, TVS was used to estimate the barrier height (Φ_B) of tunneling via a molecular junction by measuring a transition voltage (V_{trans}) required to permit a crossover from direct tunneling to Fowler−Nordheim tunneling.[14,15] Now this method is becoming a popular tool in a variety of nanostructured electronic systems such as metal−semiconductor carbon nanotube intermolecular junctions[35] and nanodielectrics for organic transistors[36] and inorganic nanowire transistors,[37] as well as in molecular electronics. Recently, TVS has also facilitated a calibration of orbital energy positions in single-molecule transistors.[6]

Moreover, the exquisite interpretation of TVS, fulfilled by comparison of the Simmons model and the coherent Landauer approach, suggests that length-dependent TVS measurements for saturated alkyl chains can provide a critical test to distinguish true molecular junctions from a vacuum tunnel junction with no molecules.[16] For this, we performed TVS on a series of alkanedithiol molecules having different lengths ranging from DC8 to DC12, employing the electromigrated nanogap junctions. Measurement of V_{trans} in the alkanedithiol junctions is illustrated in Figure 5. To generate Figure 5, representative length-dependent $I(V)$ curves displayed in the inset of Figure 5 were transformed to axes of ln(I/V^2) against $1/V$, known as a Fowler−Nordheim plot where an inflection point denotes V_{trans}

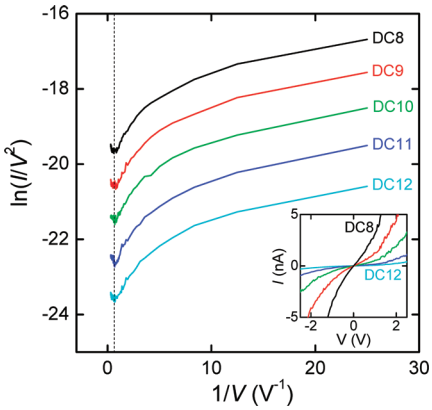

Figure 5. $\ln(I/V^2)$ versus $1/V$ curves for five different length alkanedithiols, where the vertical dashed line denotes the transition voltage (V_{trans}). The inset shows corresponding $I(V)$ curves. All data were obtained at 4.2 K.

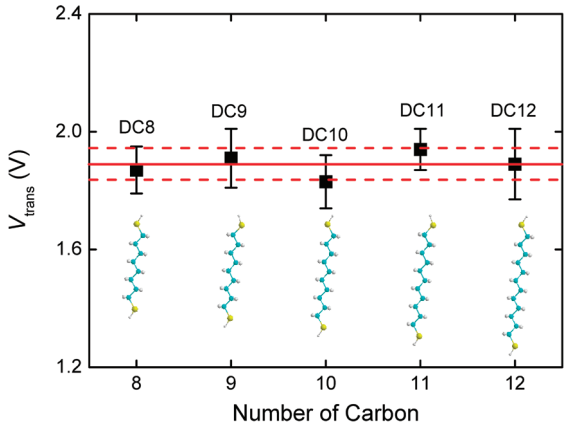

Figure 6. V_{trans} as a function of molecular length for a series of alkanedithiols from DC8 to DC12. The solid line represents the mean value of V_{trans} for five different length alkanedithiols, and two dashed lines show the standard deviation for averaging. Error bars on each data point also denote the standard deviation across individual measurements for different devices. Chemical structures for each molecule are displayed in the inset.

(as indicated by the vertical dashed line in Figure 5). V_{trans} for a series of alkanedithiol molecules is summarized graphically in Figure 6. The average value of V_{trans}, represented by the solid line in Figure 6, falls within the standard deviation (within two dashed lines) of measured values for each of the molecules, thereby illustrating that V_{trans} is invariant with molecular length for alkanedithiols. This result is consistent with the fact that the HOMO−LUMO gap of these molecules is virtually length independent, and thus agrees with the data of Beebe et al.[15] Similarly, ultraviolet photoelectron spectroscopy measurements have shown that the energy offset between the HOMO and the electrode's Fermi level for different length alkyl chains is constant.[38,39]

We note that such length constancy in V_{trans} for the alkanedithiol junctions is fully in agreement with the results expected from a coherent molecular transport model based on the Landauer formula; that is, V_{trans} is independent of molecular length (longer than ~8 Å) for constant Φ_B.[16] On the other hand, V_{trans} is expected to be inversely proportional to tunneling length for the case of a tunnel junction without molecules obeying the Simmons model.[16] Only within the coherent molecular transport picture, V_{trans} can be directly scaled with Φ_B, thus giving valid information on molecular energy levels. Therefore, our findings on length-dependent TVS measurements provide additional verification of the molecular junction formation by the electromigration.

Conclusions

In the present study, we have demonstrated the proof of intrinsic molecular transport in the electromigrated nanogap junctions using a mutiprobe approach combining a variety of transport techniques. The completely assigned IETS spectrum, the temperature-independent $I(V)$ behavior, the correct exponential decay of conductance with molecular length, and the length-dependent TVS measurements for the saturated alkyl control series all indicate the fact that we did indeed probe a molecular system in the electromigrated nanogap junctions. These results can provide stringent criteria to establish a valid molecular transport junction under a probabilistic fabrication process.

Acknowledgment. This work was supported by the Korean National Research Laboratory program, a Korean National Core Research Center grant, the World Class University program of the Korean Ministry of Education, Science and Technology of Korea, the Program for Integrated Molecular System at the Gwangju Institute of Science and Technology, the System-IC2010 project of the Korean Ministry of Knowledge Economy, the US Army Research Office (W911NF-08-1-0365), and the Canadian Institute for Advanced Research (CIfAR).

Supporting Information Available: IETS spectrum for both polarities of positive and negative bias and statistical histogram for conductance values of the alkanedithiol junctions. This material is available free of charge via the Internet at http://pubs.acs.org.

References and Notes

(1) Aviram, A.; Ratner, M. A. *Chem. Phys. Lett.* **1974**, *29*, 277.
(2) Reed, M. A.; Lee, T. *Molecular Nanoelectronics*; American Scientific: Stevenson Ranch, CA, 2003.
(3) Cuniberti, G., Fagas, G., Richter, K., Eds. *Introducing Molecular Electronics*; Springer-Verlag: Berlin, Heidelberg, 2005.
(4) Díez-Pérez, I.; Hihath, J.; Lee, Y.; Yu, L.; Adamska, L.; Kozhushner, M. A.; Oleynik, I. I.; Tao, N. *Nat. Chem.* **2009**, *1*, 635.
(5) van der Molen, S. J.; Liljeroth, P. *J. Phys.: Condens. Matter* **2010**, *22*, 133001.
(6) Song, H.; Kim, Y.; Jang, Y. H.; Jeong, H.; Reed, M. A.; Lee, T. *Nature* **2009**, *462*, 1039.
(7) Park, J.; Pasupathy, A. N.; Goldsmith, J. I.; Chang, C.; Yaish, Y.; Petta, J. R.; Rinkoski, M.; Sethna, J. P.; Abruna, H. D.; McEuen, P. L.; Ralph, D. C. *Nature* **2002**, *417*, 722.
(8) Kubatkin, S.; Danilov, A.; Hjort, M.; Cornil, J.; Brédas, J. L.; Stuhr-Hansen, N.; Per Hedegård, P.; Bjørnholm, T. *Nature* **2003**, *425*, 698.
(9) Park, H.; Lim, A. K. L.; Alivisatos, A. P.; Park, J.; McEuen, P. L. *Appl. Phys. Lett.* **1999**, *75*, 301.
(10) Wang, W.; Lee, T.; Kretzschmar, I.; Reed, M. A. *Nano Lett.* **2004**, *4*, 643.
(11) Kushmerick, J. G.; Lazorcik, J.; Patterson, C. H.; Shashidhar, R.; Seferos, D. S.; Bazan, C. G. *Nano Lett.* **2004**, *4*, 639.
(12) Galperin, M.; Ratner, M. A.; Nitzan, A.; Troisi, A. *Science* **2008**, *319*, 1056.
(13) Wang, W.; Lee, T.; Reed, M. A. *Phys. Rev. B* **2003**, *68*, 035416.
(14) Beebe, J. M.; Kim, B.; Gadzuk, J. W.; Frisbie, C. D.; Kushmerick, J. G. *Phys. Rev. Lett.* **2006**, *97*, 026801.
(15) Beebe, J. M.; Kim, B.; Frisbie, C. D.; Kushmerick, J. G. *ACS Nano* **2008**, *2*, 827.
(16) Huisman, E. H.; Guédon, C. M.; van Wees, B. J.; van der Molen, S. J. *Nano Lett.* **2009**, *9*, 3909.
(17) Tao, N. J. *Nat. Nanotechnol.* **2006**, *1*, 173.
(18) Gonzalez, J. I.; Lee, T. H.; Barnes, M. D.; Antoku, Y.; Dickson, R. M. *Phys. Rev. Lett.* **2004**, *93*, 147402.
(19) Sordan, R.; Balasubramanian, K.; Burghard, M.; Kern, K. *Appl. Phys. Lett.* **2005**, *87*, 013106.
(20) Houck, A. A.; Labaziewicz, J.; Chan, E. K.; Folk, J. A.; Chuang, I. L. *Nano Lett.* **2005**, *5*, 1685.

(21) Heersche, H. B.; de Groot, Z.; Folk, J. A.; Kouwenhoven, L. P.; van der Zant, H. S. J.; Houck, A. A.; Labaziewicz, J.; Chuang, I. L. *Phys. Rev. Lett.* **2006**, *96*, 017205.
(22) Taychatanapat, T.; Bolotin, K. I.; Kuemmeth, F.; Ralph, D. C. *Nano Lett.* **2007**, *7*, 652.
(23) Luo, K.; Chae, D. H.; Yao, Z. *Nanotechnology* **2007**, *18*, 465203.
(24) Mangin, A.; Anthore, A.; Della Rocca, M. L.; Boulat, E.; Lafarge, P. *J. Appl. Phys.* **2009**, *105*, 014313.
(25) Strachan, D. R.; Smith, D. E.; Johnston, T.-H.; Therien, M. J.; Bonnell, D. A.; Johnson, A. T. *Appl. Phys. Lett.* **2005**, *86*, 043109.
(26) Horowitz, P.; Hill, W. *The Art of Electronics*; Cambridge University Press: New York, 1989.
(27) van der Zant, H. S. J.; Kervennic, Y.-V.; Poot, M.; O'Neill, K.; de Groot, Z.; Heeersche, H. B.; Stuhr-Hansen, N.; Bjørnholm, T.; Vanmaekelbergh, D.; van Walree, C. A.; Jenneskens, L. W. *Faraday Discuss.* **2006**, *131*, 347.
(28) Jaklevic, R. C.; Lambe, J. *Phys. Rev. Lett.* **1966**, *17*, 1139.
(29) Holmlin, R. E.; Haag, R.; Chabinyc, M. L.; Ismagilov, R. F.; Cohen, A. E.; Terfort, A.; Rampi, M. A.; Whitesides, G. M. *J. Am. Chem. Soc.* **2001**, *123*, 5075.
(30) Wold, D. J.; Frisbie, C. D. *J. Am. Chem. Soc.* **2001**, *123*, 5549.
(31) Wold, D. J.; Haag, R.; Rampi, M. A.; Frisbie, C. D. *J. Phys. Chem. B* **2002**, *106*, 2813.
(32) Liu, K.; Wang, X.; Wang, F. *ACS Nano* **2008**, *2*, 2315.
(33) Yu, L. H.; Gergel-Hackett, N.; Zangmeister, C. D.; Hacker, C. A.; Richter, C. A.; Kushmerick, J. G. *J. Phys.: Condens. Matter* **2008**, *20*, 374114.
(34) Choi, S. H.; Kim, B.; Frisbie, C. D. *Science* **2008**, *320*, 1482.
(35) Chiu, P. W.; Roth, S. *Appl. Phys. Lett.* **2008**, *92*, 042107.
(36) DiBenedetto, S. A.; Facchetti, A.; Ratner, M. A.; Marks, T. J. *J. Am. Chem. Soc.* **2009**, *131*, 7158.
(37) Choe, M.; Jo, G.; Maeng, J.; Hong, W. K.; Jo, M.; Wang, G.; Park, W.; Lee, B.; Hwang, H.; Lee, T. *J. Appl. Phys.* **2010**, *107*, 034504.
(38) Alloway, D. M.; Hofmann, M.; Smith, D. L.; Gruhn, N. E.; Graham, A. L.; Colorado, R., Jr.; Wysocki, V. H.; Lee, R.; Lee, P. A.; Armstrong, N. *J. Phys. Chem. B* **2003**, *107*, 11690.
(39) Duwez, A. S.; Pfister-Guillouzo, G.; Delhalle, J.; Riga, J. *J. Phys. Chem. B* **2000**, *104*, 9029.

JP104760B